Atomic and electronic structure of simple metal/graphene and complex metal/graphene/metal interfaces

Lyudmyla Adamska,[1] You Lin,[1] Andrew J. Ross,[2] Matthias Batzill,[1] and Ivan I. Oleynik[1]
[1]*Department of Physics, University of South Florida, Tampa, Florida 33620, USA*
[2]*Saint Anselm College, Manchester, New Hampshire 03102, USA*
(Received 3 February 2012; published 22 May 2012)

Structural, electronic, and magnetic properties of simple interfaces (graphene on top of a metallic substrate) and complex interfaces (a single metallic adlayer on a simple graphene/metal system, either on top or between the graphene and metallic substrate) have been studied using density functional theory. Two types of simple interface with strong (Ni/graphene) and weak (Cu/graphene) bonding were considered. In addition to binding energies and interface distances, which are used to quantify the strength of graphene-substrate interactions, the bonding in simple and complex interfaces was analyzed using charge density distributions and bond orders. Substantial enhancement of the metallic substrate/graphene binding was observed in complex interfaces, consisting of a Ni monolayer on top of a simple {Ni or Cu}/graphene interface. The increase of substrate-graphene bonding in such complex interfaces is accompanied by weakening of in-plane C-C bonds in graphene, as quantified by the bond orders. A weak ferrimagnetism in graphene, i.e., unequal magnetic moments $-0.04\mu_B$ and $+0.06\mu_B$ on the C atoms, is induced by a ferromagnetic Ni substrate. The strength of graphene-substrate interactions is also reflected in simulated scanning tunneling microscopy images.

DOI: 10.1103/PhysRevB.85.195443 PACS number(s): 61.48.Gh, 73.22.Pr, 68.65.Pq, 68.37.Ef

I. INTRODUCTION

Graphene, a one-atom-thick layer of carbon atoms, exhibits exceptional electronic properties, such as very high electron mobility, high saturation velocity, high current-carrying density, and excellent heat dissipation, which make it a highly promising material for the development of carbon-based nanoelectronics.[1–4] Graphene growth on metal substrates, including Ni,[5–10] Ru,[11–13] Pt,[14] Ir,[15–17] and Cu,[18–22] is currently a major approach for producing high-quality, large-area graphene samples for electronics applications. In addition to controlling growth processes, metal-graphene interactions influence the electronic properties of graphene. For example, a strong interfacial binding between graphene and either Ni (Refs. 6,8, and 9) or Ru (Refs. 11 and 12) substrates opens up graphene's band gap,[10,18] whereas a weak interaction with Ir (Refs. 15–17), Pt (Ref. 14), or Cu (Refs. 10,18–22) substrates preserves the electronic properties of free-standing graphene. Many proposed graphene devices contain metal/graphene electrical contacts or other metal/graphene heterostructures.[1–3] Therefore, an understanding of the fundamental properties of metal/graphene interfaces is of critical importance for developing graphene-based nanoelectronics.

Simple metal/graphene interfaces, i.e., graphene on top of a metallic substrate, have already been investigated both theoretically[10,23–25] and experimentally.[6,9,14,15,20] Khomyakov *et al.*[10] systematically studied simple metal/graphene interfaces across a wide range of metallic substrates. For a given metal, various metal/graphene stacking geometries were ranked based on calculated binding energies. By comparing the strengths of metal/graphene interactions for different metals, the interfaces were classified as strongly (Ni,Ru,Co) and weakly (Cu,Au,Pt) bonded. A new interface geometry, the so-called bridge structure, was introduced in Ref. 23. Although this geometry was later observed in experiment, it was suggested that the bridge structure appears due to pinning of graphene to the substrate by point defects.[9] It was also predicted that graphene-metal interactions reduce the metal work function, induce a shift in graphene's Dirac point in weakly bonded interfaces, and open up graphene's band gap in strongly bound interfaces.[10,26,27]

Graphene/ferromagnetic metal interfaces also play an important role in graphene-based spintronic devices. In particular, spin injection and spin transport have been achieved at room temperature in graphene-based spin valves.[28] Magnetic properties of nickel/graphene interfaces were studied both experimentally[29–31] and theoretically;[25] appreciable induced magnetic moments in carbon atoms of Ni(111)-supported graphene were found to be between $0.05\mu_B$ and $0.1\mu_B$. Even larger induced magnetic moments, $0.2\mu_B$–$0.25\mu_B$, were observed in Fe-intercalated graphene on a Ni substrate.[32,33]

Although *simple interfaces* have already attracted considerable attention,[8,10,23] *complex interfaces* consisting of a single metallic adlayer on a simple graphene/metal system, either on top or between the graphene and metallic substrate, are less understood.[7,32–35] Such complex interfaces are of particular interest in connection with experiments on intercalation of metals through graphene. For example, nickel/graphene systems, with additional intercalated metal layers, have been studied using high-resolution electron energy-loss spectroscopy;[36–41] the changes in the phonon spectra of graphene/metal systems were correlated with the modification of metal-graphene interactions by the intercalated layers. Recently it was shown that by introducing a single Au layer between strongly interacting graphene and a Ni(111) substrate, a decoupling of Ni and graphene was achieved, as evidenced by the observation of an electronic structure close to that of free-standing graphene.[34,35]

This paper systematically investigates simple (metal/graphene) and complex (metal/graphene/metal, and intercalated metal/metal/graphene) interfaces using first-principles density functional theory (DFT). Two metallic substrates, Ni

and Cu, interacting with graphene, were studied as representative cases of strongly and weakly bonded graphene/metal interfaces, respectively. In addition to binding energies and interface distances, which are used to quantify the strength of graphene-substrate interactions, the bonding in simple and complex interfaces was analyzed using charge density distributions and bond orders. The modification of interfacial atomic and electronic properties upon intercalation by the metallic (Cu or Ni) adlayer was also investigated. This research has been performed to support experiments on the growth of graphene on Ni substrates,[6,7,42] where the atomic and electronic structure was characterized primarily by scanning tunneling microscopy (STM). Therefore, STM images were simulated and analyzed to find signatures of graphene/metal interfacial interactions, thus aiding in interpretation of experimental STM images.

II. COMPUTATIONAL DETAILS

DFT calculations were performed using the linear combination of atomic orbitals (LCAO) code DMOL.[43,44] The double numerical plus polarization atomic orbital basis set was generated using a real-space cutoff of 4.0 Å. DFT semicore pseudopotentials[45] were used for the core electrons of metallic atoms, while all electrons were explicitly included for carbon atoms. The sampling of the k space was better than 0.03 $Å^{-1}$, and the convergence criterion for forces on atoms was better than 0.03 eV/Å. Spin-polarized calculations were performed for Ni substrates. The local density approximation[46] (LDA) is frequently used to study graphene on metallic substrates[6,7,10,16,25] because it predicts graphene/metal interfacial geometries in closer agreement with experiment than does the generalized gradient approximation (GGA).[47] It is well known that both the overbinding by the LDA and the underbinding by the GGA respectively result in shorter and longer bond lengths as compared to experiment. Such effects become especially pronounced in graphene/metal interfaces where weak van der Waals (vdW) interactions play a key role. Recently, several empirical vdW correction schemes were incorporated into DFT calculations,[48] the most popular being those of Grimme[49] and Tkatchenko and Scheffler (TS).[50] Both approaches are based on standard DFT with empirical vdW C_6/r^6 atom-atom pairwise contributions multiplied by damping functions to switch off diverging vdW contributions at small interatomic distances. The TS scheme is more self-consistent compared to the Grimme scheme (published[49] in 2006 and implemented in DMOL) in the sense that the C_6 coefficients are calculated using the electron density of a system under study with accurate reference data for free atoms, thus reflecting the dependence of the elemental C_6 coefficients on the local bonding environment. In the discussion below, we provide the data obtained by the TS vdW correction to the Perdew-Burke-Ernzerhof (PBE) GGA functional,[47] referred to as GGA + vdW. However, we also performed a detailed comparative study of both Grimme-2006 and TS empirical vdW schemes, and found them to produce almost indistinguishable results across all interface systems considered herein: the differences in binding energy being less than 0.01 eV/atom and in interfacial distances less than 0.01 Å.

In addition, the properties of graphene/metal interfaces were also studied using the LDA. As mentioned above, the graphene/metal interfaces were mostly studied at the LDA level before empirical vdW corrections became available in DFT codes. This is because the LDA predicts atomic structures closer to experiment than does the pure GGA. Therefore, for comparison purposes, we provide interface geometries obtained by both the LDA and GGA + vdW. In addition, the LDA was used to obtain electronic properties for the interfaces. It is well known that the LDA and GGA provide almost indistinguishable electronic structures for systems with the same geometry. However, the interface electronic structure must be simultaneously determined with the equilibrium atomic structure through minimizating the total energy of the system. Because the empirical vdW atom-atom potential does not contribute directly to the electronic structure, it would be more consistent to use the pure LDA without vdW contributions, since the LDA provides geometries close to those obtained by the GGA + vdW, while calculating the total energy using the electron density distribution, which reflects physically important chemical interactions in the system.

Most of the interfacial structures were built using 1×1 (111) fcc surface unit cells containing five (111) layers of metal (Ni or Cu) and graphene on top of a metallic slab. Interfaces with larger surface unit cells (12 times larger surface area) were used to partially relax restrictions imposed by periodic boundary conditions on small 1×1 unit cells, which may result in the elimination of some interfacial structures that otherwise would be stable in larger unit cells. The two bottom layers of the substrate were fixed during geometry optimization, all other atoms in the system being allowed to move.

A major issue in interfacial calculations is the accommodation of mismatch between the metallic substrate and graphene. In the case of Ni, the mismatch is 1.3%; in the case of Cu 3.8%. To decide whether the graphene or substrate in-plane dimensions were adjusted to match the other interface counterpart, the total energy of the combined graphene/metal system was calculated as a function of the in-plane lattice constant. In both the Ni/graphene and Cu/graphene cases, the optimal in-plane lattice constant was closer to that of the metal. Therefore, in all calculations, the interfaces were built by adjusting the graphene lattice constant to match the metal (111) in-plane lattice constant derived from the theoretical bulk lattice parameter. There is a wide variety of schemes for lattice mismatch accommodation employed in several DFT calculations of metal/graphene interfaces, which makes it difficult to compare results obtained by different groups. For example, in Refs. 6, 7, and 9 graphene was stretched to match the substrate, whereas in Ref. 10 the lattice constant of the metallic substrate was adjusted to that of graphene; some authors used the experimental (unrelaxed) lattice constant.[22,23] It turned out that the lattice mismatch accommodation scheme influences the energy difference between structures with different stacking geometries. Therefore, different lattice matching schemes may produce interfaces with different interfacial geometries.[10,22,23]

III. RESULTS AND DISCUSSION

A. Atomic structure of simple metal/graphene interfaces

Although adsorption of graphene on metal surfaces was considered in several previous publications,[9,10,22,23,25–27] the

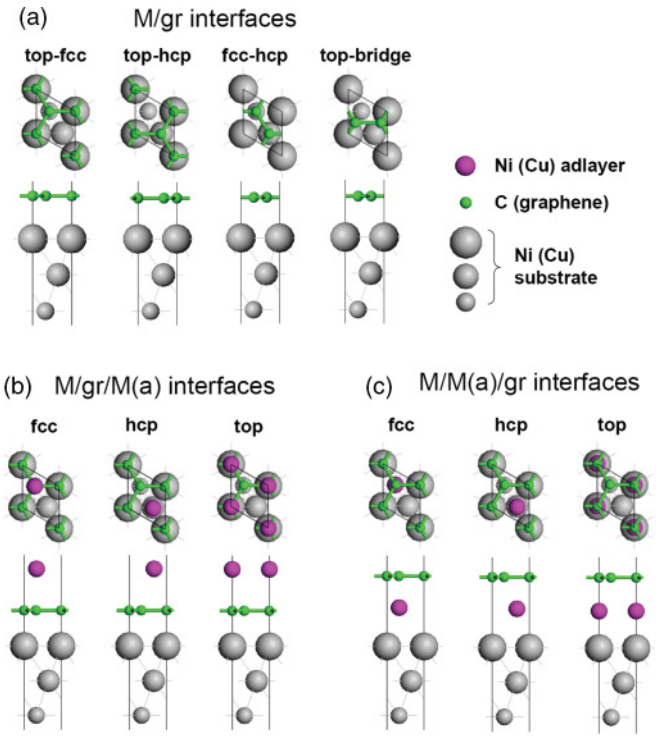

FIG. 1. (Color online) (a) Geometries of simple graphene/metal interfaces: top-fcc, top-hcp, fcc-hcp, and top-bridge. The top-fcc interface was found to be the lowest-energy configuration. (b),(c) Geometries of complex metal(s)/graphene/metal interfaces: fcc, hcp, top. See the labeling convention in the text. The fcc interface was found to be the lowest-energy structure.

geometries of simple metal/graphene interfaces were systematically investigated to fully account for the specific lattice mismatch accommodation scheme employed in this work. Four possible interface geometries were identified as top-fcc, top-hcp, fcc-hcp, and top-bridge, which describe the arrangement of two carbon atoms of a graphene unit cell with respect to the underlying structure of the metallic substrate: top, the first C atom on top of every surface metal atom; fcc and hcp, the second C atom in the hollow position above the fcc or hcp site of the (111) fcc lattice; top-bridge, one C atom between the top and fcc sites and another between the top and hcp sites. See Fig. 1(a). These interfacial structures were optimized using both the LDA and GGA + vdW, and ranked based on the strength of the metal/graphene interaction; see Table I. It was found that both the LDA and GGA + vdW give consistent results, i.e., they predict top-fcc and top-hcp interfaces as the lowest-energy structures for both Ni and Cu substrates, the top-fcc interface being only slightly lower in energy than the top-hcc interface. Although the top-bridge interface has a binding energy close to that of both top-fcc and top-hcp interfaces—in agreement with previous DFT calculations[9,23]—additional investigation of the stability of all four interfaces using substantially larger surface unit cells revealed that the top-bridge structure was unstable, i.e., eventually relaxed to the top-fcc structure, whereas all other interfaces remained stable.

The metal/graphene interlayer distances and binding energies for all four interfaces are reported in Table I. Both the GGA + vdW and LDA predict strong Ni/graphene (Ni/gr) and weak Cu/graphene (Cu/gr) interfacial bonding, as evidenced by the corresponding binding energies reported in Table I. As a consequence of the weak Cu-graphene interaction, which is also reflected in the absence of any specific metal/graphene stacking preference, the graphene layer is almost decoupled from the metallic substrate.

B. Atomic structure of complex metal/graphene interfaces

It was shown in the previous section that the simple top-fcc metal/graphene interface is the lowest-energy structure for both Ni and Cu substrates. Therefore, this specific simple interface was used to build a complex interface by positioning an additional metallic adlayer $M(a)$ either above or below graphene, thus producing M/gr/$M(a)$ or $M/M(a)$/gr interfaces. In the case of the M/gr/$M(a)$ interface, the metallic adlayer was placed on the substrate-supported graphene in three ways such that the metal atom of the metallic adlayer occupies either the top, hcp, or fcc sites of the (111) surface unit cell of the substrate; see Fig. 1(b).

The geometry of the M/gr/$M(a)$ interfaces was determined using the LDA and GGA + vdW, both methods showing that the fcc complex interface is the lowest-energy structure. The intercalated $M/M(a)$/gr interfaces were built starting from the top, fcc, and hcp structures of the M/gr/$M(a)$ interface [see Fig. 1(c)] and interchanging the graphene and metal adlayer while preserving the lateral positions of the atoms. The stacking of graphene with respect to the substrate in the initial fcc M/gr/$M(a)$ structure is top-fcc, but after interchanging the graphene and metal adlayer, it became the top-hcp $M/M(a)$/gr

TABLE I. Properties of simple metal/graphene interfaces: binding energy E_b and interface distance $d_{M\text{-gr}}$.

		GGA + vdW		LDA	
System	Stacking	E_b (eV)	$d_{M\text{-gr}}$ (Å)	E_b (eV)	$d_{M\text{-gr}}$ (Å)
Ni/gr	top-fcc	0.11	2.12	0.36	2.04
	top-hcp	0.09	2.14	0.34	2.05
	fcc-hcp	0.03	3.76	0.10	3.24
	top-bridge	0.02	2.65	0.35	1.99
Cu/gr	top-fcc	0.03	3.46	0.15	2.31
	top-hcp	0.03	3.46	0.13	2.82
	fcc-hcp	0.02	3.70	0.10	3.20
	top-bridge	0.03	3.49	0.12	2.84

TABLE II. Properties of complex metal/graphene interfaces: binding energies E_b and interface distances d. The three-layer system is labeled as $X/Y/Z$ where X is always the metallic substrate, and Y and Z graphene (gr) and metallic adlayer or vice versa. Such labeling allows the inclusion of both $M/M(a)$/graphene intercalated interfaces and M/gr/$M(a)$ interfaces with a metallic adlayer $M(a)$ on top of simple metal/graphene interfaces. Only the lowest-energy structures are shown in the table.

	GGA + vdW				LDA			
System	$X(s)/Y$ interface		Y/Z interface		$X(s)/Y$ interface		Y/Z interface	
$X(s)/Y/Z$	E_b (eV)	d (Å)	E_b (eV)	d (Å)	E_b (eV)	d (Å)	E_b (eV)	d (Å)
Ni/Ni(a)/gr	1.49	2.04	0.10	2.14	1.81	1.99	0.34	2.06
Ni/gr/Ni(a)	0.86	2.03	0.88	2.03	1.25	1.98	1.28	1.97
Ni/Cu(a)/gr	0.96	2.09	0.03	3.55	1.35	2.02	0.12	2.97
Ni/gr/Cu(a)	0.14	2.12	0.04	3.34	0.40	2.04	0.13	2.83
Cu/Cu(a)/gr	0.90	2.09	0.03	3.41	1.29	2.01	0.13	2.39
Cu/gr/Cu(a)	0.03	3.36	0.04	3.38	0.20	2.28	0.17	2.76
Cu/Ni(a)/gr	1.34	2.07	0.25	2.07	1.65	2.0	0.45	2.01
Cu/gr/Ni(a)	0.04	3.39	0.26	3.25	0.62	2.14	1.01	1.97

structure. In addition, the $M/M(a)$/gr interface, which has fcc adlayer stacking, preserves the standard a-b-c-a (111) layer sequence of the fcc lattice in the composite $M/M(a)$ substrate. Therefore, it was observed that all other intercalated interfaces, i.e., hcp and top, were higher in energy. This was expected because they contain stacking faults at the $M/M(a)$ interface. In fact, the DFT geometry relaxation of all three types of interface confirmed that fcc stacking is the lowest-energy geometry for $M/M(a)$/gr interfaces.

It is evident from a comparison of Tables I and II that nearest-neighbor $M(a)$-graphene interactions dominate bonding at the interface: the binding energy and the interplanar distance for a particular $M/M(a)$/gr interface are close to those for simple M/gr interfaces, under the condition that graphene is in contact with the same type of metal, Ni or Cu. For example, the Ni/Cu(a)/gr interface displays a weak interfacial binding ($E_b = 0.03$ eV; $d = 3.55$ Å), very similar to that observed for simple Cu/gr interfaces ($E_b = 0.03$ eV; $d = 3.46$ Å), whereas adlayer-graphene interactions in the Cu/Ni(a)/gr interface are strong ($E_b = 0.25$ eV; $d = 2.07$ Å), i.e., similar to those in simple Ni/gr interfaces ($E_b = 0.09$ eV; $d = 2.12$ Å). See Tables I and II.

Following the same idea for the dominance of nearest-neighbor interactions, it would be reasonable to expect the strength of (metal-adlayer)-graphene interfacial interactions in M/gr/$M(a)$ structures to be similar to those in simple M/gr interfaces. Indeed, such a trend is present in the case of the Cu adlayer, where a weak Cu-graphene interaction is dominant in the complex Ni/gr/Cu(a) and Cu/gr/Cu(a) interfaces. Surprisingly, a strong enhancement of local Ni-graphene bonding was observed in the case of Ni/gr/Ni(a) and Cu/gr/Ni(a) complex interfaces, for which a Ni adlayer was deposited onto Ni-supported or Cu-supported graphene. In particular, the binding energy of 0.11 eV in the simple Ni/graphene interface was increased to 0.87 eV for both (Ni-substrate)-graphene and graphene-(Ni-adlayer) interactions in the Ni/gr/Ni(a) complex interface. Although in the complex Cu/gr/Ni(a) interface the (Cu-substrate)-graphene interaction was not affected by the addition of the Ni adlayer on top of graphene, the graphene-Ni(a) interaction was enhanced from 0.1 to 0.26 eV. A close inspection of the interface geometry of the Ni/gr/Ni(a) complex interface revealed a strong buckling of the graphene layer with a corrugation amplitude of 0.31 Å, accompanied by changes of in-plane C-C-C (from 120° to 115.4°) and out-of-plane Ni-C-C (90° to 102.4°) angles (see Fig. 2), which demonstrates the transition from sp^2 to sp^3 hybridization of graphene C atoms. Similar but smaller changes in interface geometry were also detected for the Cu/gr/Ni(a) interface: Ni-C-C and Cu-C-C angles were found to be 99.5°, the C-C-C angle 117.3°, and the corrugation amplitude 0.24 Å. The change of C-atom hybridization upon adsorption of a metal cluster on top of metal-supported graphene was first observed by Feibelman.[16]

C. Bond-order analysis of interfacial interactions

The LCAO basis set used in DMOL is particularly suited for the calculation of bond orders, the nondiagonal elements of the electron density matrix that characterize the strength of individual bonds. The quantitative analysis of metal/graphene interfacial bonding was performed by evaluating Mayer's bond orders[51] within the LDA. See Table III. In particular, the bond orders in simple Ni-graphene and Cu-graphene interfaces showed that the Ni-C interfacial bond is substantially stronger than the Cu-C bond; see Table III. Bond-order analysis also confirms the local nature of interfacial bonding: the Ni-C bonds in both simple Ni/graphene and complex Ni/graphene/Cu(a) interfaces are of the same strength as the Cu-C bonds in Cu/graphene and Cu/graphene/Cu(a) interfaces; see Table III. A substantial enhancement of substrate-graphene bonding

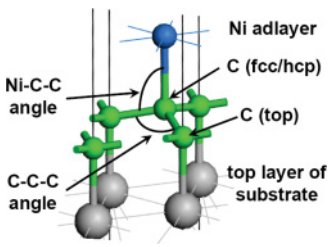

FIG. 2. (Color online) Geometry of complex Ni/graphene/Ni(a) interface: transition from sp^2 to sp^3 hybridization of graphene C atoms.

TABLE III. Mayer's bond orders for interfacial metal-carbon and graphene's carbon-carbon bonds in simple and complex interfaces, as well as carbon-carbon bond orders in free-standing graphene.

System	Ni-C	C-Ni(a)	Cu-C	C-Cu(a)	C-C
Graphene					1.21
Ni/gr	0.33				1.08
Ni/Cu(a)/gr				0.0	1.18
Ni/gr/Cu(a)	0.36			0.0	1.06
Ni/gr/Ni(a)	0.56	0.64			0.97
Cu/gr			0.20		1.13
Cu/Ni(a)/gr		0.40			1.06
Cu/gr/Ni(a)		0.62	0.38		0.98
Cu/gr/Cu(a)			0.22	0.0	1.10

occurs upon adsorption of a Ni adlayer on top of both Ni/graphene and Cu/graphene interfaces. In the particular case of a Ni-graphene-Ni complex interface, one might think of increasing strength for interfacial graphene-Ni bonding due to an additional direct interaction between the metal surfaces sandwiching graphene. The existence of such further nearest-neighbor interactions is ruled out by the bond-order analysis, indicating that binding enhancement is due to complex changes in the electronic structure of the entire interfacial system upon the adsorption of an adlayer on top of the interface.

Another interesting observation was that the strength of in-plane C-C bonds in graphene is affected by interfacial metal-graphene interactions. The bond order 1.21 in free-standing graphene is reduced to 1.08 and 1.13 upon interaction with Ni and Cu substrates, respectively; see Table III. The C-C in-plane bonds are appreciably modified upon the addition of a Ni adlayer to the simple Ni-graphene interface; the C-C bond order is further reduced to 0.97, which is due to the sp^2 to sp^3 hybridization change for the graphene C atoms.

D. Induced magnetism in graphene

Because of the ferromagnetic nature of the Ni substrate, nickel-graphene interface interactions are expected to modify the surface magnetic properties of the Ni substrate and induce magnetism in graphene. In fact, a reduction in magnetic moment for surface nickel atoms upon graphene adsorption was first predicted by theory[25] and later found in experiments by Dedkov *et al.*.[29] In our calculations of the simple Ni/graphene interface in the lowest top-fcc configuration, a substantial decrease in Ni magnetic moment of the topmost Ni layer interacting with graphene was found, from $0.71\mu_B$ to $0.47\mu_B$, which is in good agreement with experiment, from 0.72 μ_B to 0.52 μ_B.[29] In addition, the two carbon atoms of the graphene unit cell acquire magnetic moments $-0.044\mu_B$ and $+0.064\mu_B$. The opposite directions of the magnetic moments indicate the ferrimagnetic nature of the magnetic interactions at a simple Ni-graphene interface. The induced ferrimagnetism in graphene is substantially reduced in the complex Ni/graphene/Ni(a) interface upon adsorption of a Ni adlayer, the magnetic moments on C atoms being $-0.018\mu_B$ and $+0.009\mu_B$. This is in line with our previous observation of substantial changes in interfacial metal-graphene interactions upon deposition of a Ni adlayer on top of a simple Ni-graphene interface. Interestingly, the induced magnetic moments on C atoms remain intact upon adsorption of a Cu adlayer on top of a simple Ni-graphene structure, which confirms our earlier conclusion about the decoupling of the graphene and the Cu adlayer. Intercalation of the Cu layer underneath the graphene completely turns off the induced magnetism in graphene. Both simple and complex interfaces containing a Cu substrate do not display magnetism, even in the complex Cu-graphene-Ni(a) structure. The induced magnetism in graphene adsorbed on top of a Ni substrate was also observed recently in an experiment by Dedkov and co-workers,[30,31] who measured induced magnetic moments between $0.05\mu_B$ and $0.1\mu_B$ per carbon atom.

E. Charge density distribution at the interface

The different strengths of metal-graphene bonding are also correlated with a varying degree of electron density localization along carbon-metal bonds. In fact, our calculations demonstrate a substantial electron charge localization along Ni-C bonds, which independently confirms the strong interface interaction of graphene with a Ni substrate in simple Ni/gr interfaces. See Fig. 3(a). Evidently, the very weak graphene-copper interaction corresponds to a negligibly small degree of overlap of electronic densities from C atoms of graphene and Cu atoms of the substrate; see Fig. 3(b). As shown above, the nearest-neighbor graphene-metal interactions dominate the interface bonding in complex interfaces, with the exception of systems containing a Ni adlayer. This conclusion is nicely illustrated using electron density distributions across the interface. For example, nearly identical electron density patterns with strong C-Ni overlaps are displayed in Figs. 3(a) and 3(d), which correspond to strongly interacting complex Cu/Ni(a)/gr and simple Ni/gr interfaces. This is in line with the almost identical Ni-graphene distances and binding energies for these two interfaces; see Table II. A weak Cu-graphene interaction in the complex Ni/Cu(a)/gr interface corresponds to zero overlap of electron densities as is seen in Fig. 3(e). Such a charge distribution is similar to that in a simple Cu/gr interface in the top-hcp configuration; see Fig. 3(c), which was specifically considered here to match the stacking of atomic layers in both interfaces.

Substantial bonding enhancement upon the addition of a Ni adlayer to a simple Ni/gr interface is also evident from the electron density distribution across the interface. Figure 3(f) displays the enhancement of electron density localization along both Ni-graphene and graphene-Ni(a) bonds, which results in strengthening of the interfacial bonding and a transition from sp^2 to sp^3 hybridization of graphene's carbon atoms. A similar, but considerably weaker, increase of interface binding was also observed in the Cu/gr/Ni(a) complex interface; see Fig. 3(h). In contrast, the addition of a Cu adlayer to both Ni/gr and Cu/gr simple interfaces has no effect on interface bonding as is evidenced by the zero overlap of charge density between the Cu adlayer and graphene. See Figs. 3(g) and 3(i).

F. STM images of graphene on Ni and Cu surfaces

Due to its intrinsic capability to probe the surface electronic structure, scanning tunneling microscopy can be used to

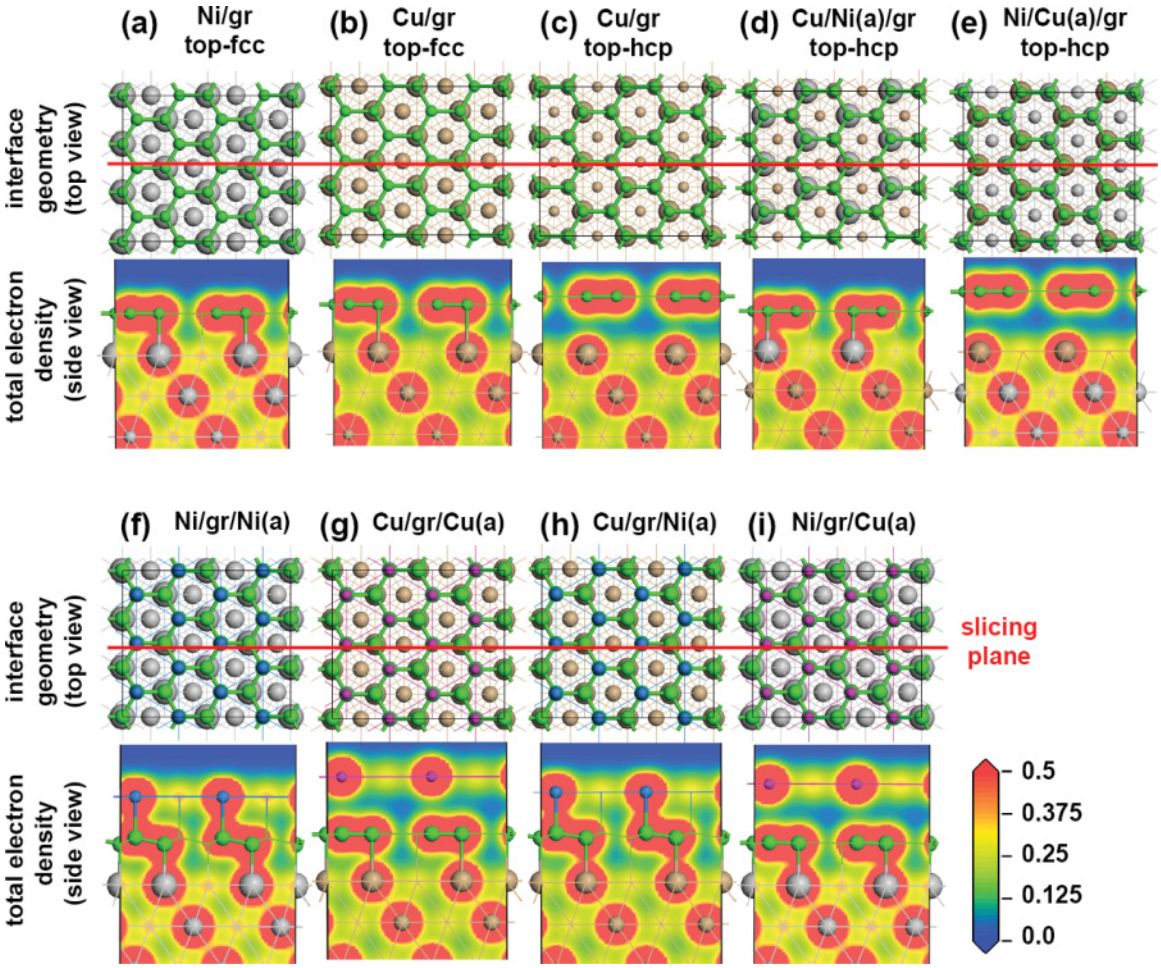

FIG. 3. (Color online) Charge density distribution across M/gr, $M/M(a)$/gr and M/gr/$M(a)$ interfaces. The red line indicates the position of the vertical slicing plane for plotting electron density.

characterize both the geometry and the strength of metal/graphene interactions via real-space imaging of electronic density at the atomic scale.[52,53] In this work, STM images were simulated using the Tersoff-Hamman approach.[54] The STM image of free-standing graphene, Fig. 4(a), displays each carbon atom, whereas the STM images of Ni/graphene interfaces in fcc [Fig. 4(b)] and hcp [Fig. 4(c)] stacking geometries display every second carbon atom of graphene in threefold fcc [Fig. 4(b)] or hcp [Fig. 4(c)] hollow sites, which do not directly bond with the Ni atoms of the surface layer of the substrate. Such suppression of the contributions of the carbon atoms directly interacting with the atoms of the substrate is similar to that in STM images of graphite in Bernal stacking,[55] where every second atom not participating in interlayer binding is visible. This feature of the STM image, displaying carbon atoms at fcc or hcp hollow sites of strongly interacting Ni-graphene interfaces, was the key for the successful indentification of a topological line defect in graphene grown on a Ni substrate.[42] In contrast, the STM images of graphene weakly interacting with Cu for both fcc and hcp stacking geometries are very close to that of free-standing graphene: each carbon atom is clearly visible as a bright spot. The STM images of graphene on Ni and Cu substrates simulated in this work, clearly reflecting the strength of graphene-metal interactions, are in good agreement with experimental STM observations.[20,42]

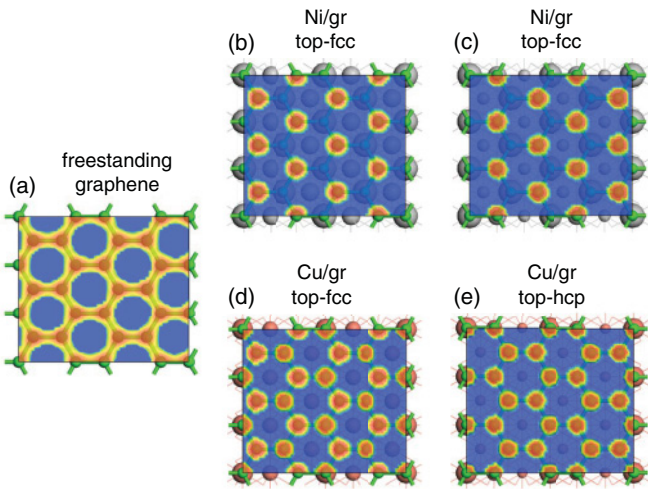

FIG. 4. (Color online) STM images simulated using Tersoff-Hamman approach: (a) free-standing graphene; (b) top-fcc Ni/gr interface; (c) top-hcp Ni/gr interface; (d) top-fcc Cu/gr interface; (e) top-hcp Cu/gr interface. The bias voltage for (a)–(c) is 100 mV; for (d) and (e) 200 mV.

IV. CONCLUSIONS

Structural, electronic, and magnetic properties of simple and complex graphene/Ni(111) and graphene/Cu(111) interfaces relevant to experimental studies of graphene growth on metallic substrates were investigated using DFT. The top-fcc stacking of simple graphene/Ni(111) and graphene/Cu(111) interfaces was found to be the lowest-energy configuration, closely followed by the top-hcp configuration, thus explaining the experimental observation of a topological line defect in graphene grown on a Ni(111) surface.[42] Substantial enhancement of the metallic substrate/graphene binding was observed in complex interfaces, consisting of a Ni monolayer on top of a simple {Ni or Cu}/graphene interface. The increase of substrate-graphene bonding in complex interfaces is accompanied by weakening in-plane C-C bonds in graphene, as quantified by the bond orders. This weakening of in-plane carbon bonds may explain the thermal instability of graphene if sandwiched between two Ni layers.[56] The structure and bonding of simple and complex interfaces were investigated using calculated electron charge density distributions and bond orders at the interface. A weak ferrimagnetism is induced in graphene upon adsorption on Ni(111). The calculated STM images contain signatures of strong and weak graphene-metal interactions in Ni/graphene and Cu/graphene interfaces, respectively. The basic information on metal/graphene interfaces obtained in this work is useful for developing optimized strategies for epitaxial growth of graphene on metallic substrates, as well as for fabrication of robust metal/graphene contacts in graphene nanoelectronic devices.

ACKNOWLEDGMENTS

This work has been supported by NSF (Grant No. EMT-0726842) and ONR (Grant No. N00014-10-1-0668) L.A. has been supported by a USF Presidential Fellowship Grant. A.J.R. has been supported by the NSF REU program (Grant No. DMR-1004873). Calculations were performed using the NSF TeraGrid facilities, the USF Research Computing Cluster, and the computational facilities of the Materials Simulation Laboratory at USF.

[1] 1. K. S. Novoselov, A. K. Geim, S. V. Morozov, D. Jiang, Y. Zhang, S. V. Dubonos, I. V. Grigorieva, and A. A. Firsov, Science **306**, 666 (2004).
[2] P. Avouris, Nano Lett. **10**, 4285 (2010).
[3] F. Schwierz, Nat. Nanotechnol. **5**, 487 (2010).
[4] F. Xia, V. Perebeinos, Y.-M. Lin, Y. Wu, and P. Avouris, Nat. Nanotechnol. **6**, 179 (2011).
[5] M. Batzill, Surf. Sci. Rep. **67**, 83 (2012).
[6] J. Lahiri, T. Miller, L. Adamska, I. I. Oleynik, and M. Batzill., Nano Lett. **11**, 518 (2011).
[7] J. Lahiri, T. S. Miller, A. J. Ross, L. Adamska, I. I. Oleynik, and M. Batzill.New J. Phys. **13**, 025001 (2011).
[8] Yu. S. Dedkov and M. Fonin, New J. Phys. **12**, 125004 (2010).
[9] W. Zhao, S. M. Kozlov, O. Höfert, K. Gotterbarm, M. P. A. Lorentz, F. Viñes, C. Papp, A. Görling, and H.-P. Steinrück, J. Phys. Chem. Lett.**2**, 759 (2011).
[10] P. A. Khomyakov, G. Giovannetti, P. C. Rusu, G. Brocks, J. van den Brink, and P. J. Kelly, Phys. Rev. B **79**, 195425 (2009).
[11] S. Marchini, S. Gunther, and J. Wintterlin, Phys. Rev. B **76**, 075429 (2007).
[12] D. Martoccia, P. R. Willmott, T. Brugger, M. Bjorck, S. Gunther, C. M. Schleputz, A. Cervellino, S. A. Pauli, B. D. Patterson, S. Marchini, J. Wintterlin, W. Moritz, and T. Greber, Phys. Rev. Lett. **101**, 126102 (2008).
[13] B. Wang, S. Günter, J. Wintterlin, and M.-L. Bocquet, New J. Phys. **12**, 043041 (2010).
[14] P. Sutter, J. T. Sadowski, and E. Sutter, Phys. Rev. B **80**, 245411 (2009).
[15] A. T. NDiaye, S. Bleikamp, P. J. Feibelman, and T. Michely, Phys. Rev. Lett. **97**, 215501 (2006).
[16] P. J. Feibelman, Phys. Rev. B **77**, 165419 (2008).
[17] I. Pletikosic, M. Kralj, P. Pervan, R. Brako, J. Coraux, A. T. NDiaye, C. Busse, and T. Michely, Phys. Rev. Lett. **102**, 056808 (2009).
[18] C. Gong, G. Lee, B. Shan, E. M. Vogel, R. M. Wallace, and K. Cho, J. Appl. Phys. **108**, 123711 (2010).
[19] S. Bae, H. Kim, Y. Lee, X. Xu, J.-S. Park, Y. Zheng, J. Balakrishnan, T. Lei, H. R. Kim, Y. II Song, Y.-J. Kim, K. S. Kim, B. Özyilmaz, J.-H. Ahn, B. H. Hong, and S. Iijima, Nat. Nanotechnol. **5**, 574 (2010).
[20] L. Gao, J. R. Guest, and N. P. Guisinger, Nano Lett. **10**, 3512 (2010).
[21] I. Jeon, H. Yang, S.-H. Lee, J. Heo, D. H. Seo, J. Shin, U-I. Chung, Z. G. Kim, H.-J. Chung, and S. Seo, ACS Nano **5**, 1915 (2011).
[22] Z. Xu and M. J. Buehler, J. Phys.: Condens. Matter **22**, 485301 (2010).
[23] M. Fuentes-Cabrera, M. I. Baskes, A. V. Melechko, and M. L. Simpson, Phys. Rev. B **77**, 035405 (2008).
[24] G. Giovannetti, P. A. Khomyakov, G. Brocks, P. J. Kelly, and J. van den Brink, Phys. Rev. B **76**, 073103 (2007).
[25] G. Bertoni, L. Calmels, A. Altibelli, and V. Serin, Phys. Rev. B **71**, 075402 (2005).
[26] G. Giovannetti, P. A. Khomyakov, G. Brocks, V. M. Karpan, J. van den Brink, and P. J. Kelly, Phys. Rev. Lett. **101**, 026803 (2008).
[27] P. A. Khomyakov, A. A. Starikov, G. Brocks, and P. J. Kelly, Phys. Rev. B **82**, 115437 (2010).
[28] N. Tombros, C. Jozsa, M. Popinciuc, H. T. Jonkman, and B. J. van Wees, Nature (London) **448**, 571 (2007).
[29] Yu.S. Dedkov, M. Fonin, and C. Laubschat, Appl. Phys. Lett. **92**, 052506 (2008).
[30] Yu. S. Dedkov, M. Sicot, and M. Fonin, J. Appl. Phys. **107**, 09E121 (2010).
[31] M. Weser, Y. Rehder, K. Horn, M. Sicot, M. Fonin, A. B. Preobrajenski, E. N. Voloshina, E. Goering, and Yu. S. Dedkov, Appl. Phys. Lett. **96**, 012504 (2010).
[32] M. Weser, E. N. Voloshina, K. Horn, and Yu. S. Dedkov, Phys. Chem. Chem. Phys. **13**, 7534 (2011).
[33] X. Sun, A. Pratt, and Y. Yamauchi, J. Phys. D **43**, 385002 (2010).

[34] A. Varykhalov, J. Sanchez-Barriga, A. M. Shikin, C. Biswas, E. Vescovo, A. Rybkin, D. Marchenko, and O. Rader, Phys. Rev. Lett. **101**, 157601 (2008).
[35] M. H. Kang, S. C. Jung, and J. W. Park, Phys. Rev. B **82**, 085409 (2010).
[36] Yu. S. Dedkov, A. M. Shikin, V. K. Adamchuk, S. L. Molodtsov, C. Laubschat, A. Bauer, and G. Kaindl, Phys. Rev. B **64**, 035405 (2001).
[37] A. M. Shikin, D. Farías, and K. H. Rieder, Europhys. Lett. **44**, 44 (1998).
[38] D. Farías, A. M. Shikin, K.-H. Rieder, Yu. S. Dedkov, J. Phys.: Condens. Matter **11**, 8453 (1999).
[39] A. M. Shikin, G. V. Prudnikova, V. K. Adamchuk, F. Moresco, and K.-H. Rieder, Phys. Rev. B **62**, 13202 (2000).
[40] D. Farías, K. H. Rieder, A. M. Shikin, V. K. Adamchuk, T. Tanaka, and C. Oshima, Surf. Sci. **454–456**, 437 (2000).
[41] A. M. Shikin, D. Farías, V. K. Adamchuk, and K.-H. Rieder, Surf. Sci. **424**, 155 (1999).
[42] J. Lahiri, Y. Lin, P. Bozkurt, I. I. Oleynik, and M. Batzill, Nat. Nanotechnol. **5**, 326 (2010).
[43] B. Delley, J. Chem. Phys. **92**, 508 (1990).
[44] B. Delley, J. Chem. Phys. **113**, 7756 (2000).
[45] B. Delley, Phys. Rev. B **66**, 155125 (2002).
[46] J. P. Perdew and A. Zunger, Phys. Rev. B **23**, 5048 (1981).
[47] J. P. Perdew, K. Burke, and M. Ernzerhof, Phys. Rev. Lett. **77**, 3865 (1996).
[48] A. Tkatchenko, L. Romaner, O. T. Hofmann, E. Zojer, C. Ambrosch-Draxl, and M. Scheffler, MRS Bull. **35**, 435 (2010).
[49] S. Grimme, J. Comput. Chem. **27**, 1787 (2006).
[50] A. Tkatchenko and M. Scheffler, Phys. Rev. Lett. **102**, 073005 (2009).
[51] I. Mayer, Chem. Phys. Lett. **97**, 270 (1983).
[52] J. Chen, *Introduction to Scanning Tunneling Microscopy* (Oxford University Press, Oxford, 1993).
[53] R. Wiesendanger, *Scanning Probe Microscopy and Spectroscopy: Methods and Applications* (Cambridge University Press, Cambridge, 1994).
[54] J. Tersoff and D. R. Hamann, Phys. Rev. B **31**, 805 (1985).
[55] I. P. Batra, N. García, H. Rohrer, H. Salemink, E. Stoll, and S. Ciraci, Surf. Sci. **181**, 126 (1987).
[56] J. Lahiri and M. Batzill, Appl. Phys. Lett. **97**, 023102 (2010).